SCIENCE CHINA
Technological Sciences

•Article•

January 2020 Vol.63 No.1: 155–165
https://doi.org/10.1007/s11431-019-9559-2

Integrated energy-oriented cruising control of electric vehicle on highway with varying slopes considering battery aging

ZHUANG WeiChao[1], QU LingHu[1], XU ShaoBing[2], LI BingBing[1], CHEN Nan[1] & YIN GuoDong[1*]

[1] *School of Mechanical Engineering, Southeast University, Nanjing 211189, China;*
[2] *Department of Mechanical Engineering, University of Michigan, Ann Arbor 48105, USA*

Received January 7, 2019; accepted August 12, 2019; published online November 8, 2019

Eco-driving strategies for vehicles with conventional powertrains have been studied for years and attempt to reduce fuel consumption by optimizing the driving velocity profile. For electric vehicles (EVs) with regenerative braking, the speed profile with the best energy efficiency should be different from conventional vehicles. This paper proposes an energy-oriented cruising control strategy for EVs with a hierarchical structure to realize eco-cruising on highways with varying slopes. The upper layer plans the energy-optimized vehicle velocity, and the lower layer calculates the torque allocation between the front and rear axles. However, the resulting speed profile with varying velocity may cause a high charge and discharge rate of the battery, resulting in rapid battery fading. To extend the battery life, we make a tradeoff between the energy consumption and wear of the battery by formulating an optimal control problem, where driving comfort and travel time are also considered. An indirect optimal control method is implemented to derive the optimal control rule. As an extension, the control rule for avoiding rear-end collisions is presented and simulated for driving in the real world.

eco-driving, electric vehicle, battery fading model, dynamic programming, energy management

Citation: Zhuang W C, Qu L H, Xu S B, et al. Integrated energy-oriented cruising control of electric vehicle on highway with varying slopes considering battery aging. Sci China Tech Sci, 2020, 63: 155–165, https://doi.org/10.1007/s11431-019-9559-2

1 Introduction

Tightening fuel economy and emission regulations are forcing automakers around the world to develop technologies to improve the energy efficiency of their vehicles [1]. Hybrid/electric vehicle (HEV/EV) technologies are one of the solutions that have been widely investigated and show great potential in terms of energy savings [2–4]. Recently, the emergence of connected and automated vehicles (CAVs) has provided another way to further improve the energy efficiency of ground transportation. By using the installed sensors and communication devices, a CAV can obtain look-ahead traffic information and then optimize its dynamics or cooperate with surrounding vehicles to reduce energy consumption [5–7].

One technique for improving the energy efficiency of CAVs is eco-driving, which is a vehicle longitudinal control algorithm that operates vehicles in the most energy-efficient manner by optimizing the driving speed profile [8]. Usually, the problem of obtaining the most energy-efficient speed profile is formulated as an optimal control problem. Many studies in this field focus on designing the energy-optimal controller in cruising scenarios since cruising represents a significant portion of daily driving. For example, the pulse-and-glide (PnG) strategy has been proposed for conventional vehicles with internal combustion engines, therein claiming a 20% fuel economy improvement over constant speed (CS) cruising on flat urban roads [9,10]. However, in the real

*Corresponding author (email: ygd@seu.edu.cn)

world, the road slopes cannot be ignored during cruising and will affect the optimized speed profile.

A wide variety of eco-cruising control strategies for varying slopes have been developed and can be categorized into three types: global optimization, look-ahead control and instantaneous optimization. A typical global optimal control strategy, dynamic programming (DP), has been used to numerically derive the energy-optimized speed profile [11,12]. The strategy could guarantee the optimality of the resulting speed profile; however, its computational burden prevents its real-time implementation. Iterative dynamic programming (IDP) has been recently presented to reduce the computational effort of DP; however, its real-time performance remains a problem [13]. Pontryagin's maximum principle (PMP) is another approach that analytically solves the global optimization problem [14,15]. Faster computation than DP can be achieved; however, the optimality of the results is lost due to the model simplification and assumption of constant costates. In addition to the computation time, requirements of prior knowledge of the driving information, or even the entire driving cycle, also prevent global optimization techniques from being implementing in real time directly since the traffic state is time varying. As an alternative solution, many studies have used model predictive control (MPC), also called look-ahead control, to achieve eco-cruising control [16,17]. For example, Kohut et al. [18] and Kamal et al. [19] both proposed an eco-cruising controller to minimize fuel consumption based on road gradient conditions. Kohut et al. [18] used DP to calculate the sequence of control inputs required in the prediction horizon, while Kamal et al. [19] adopted the C/GMRES method. In addition, PMP is also used to solve the MPC problem while incorporating information about more than one vehicle ahead [20]. Even if fast computations can be achieved in the future, the computation speed still poses challenges to on-board implementations.

To achieve fast eco-cruising control, an instantaneous optimization problem is formulated by introducing an equivalent conversion factor between the kinetic energy of the vehicle body and the fuel consumption of the engine [21]. By converting the vehicle kinetic energy into fuel consumption, the vehicle control inputs can be generated instantaneously by minimizing the energy consumption locally. The instantaneous optimization method yields control laws whereby each step can be computed at the level of one millisecond, making them suitable for online implementation; however, its optimality has not yet been proven.

The above-mentioned studies all focused on the eco-cruising control of conventional vehicles. In addition to conventional vehicles, the energy efficiency of HEV/EVs can also be improved by planning their speed properly [22,23]. Since HEV/EVs can recover energy from regenerative braking, Xu et al. [24] and Wu et al. [25] both showed different driving patterns than conventional vehicles. To avoid over-discharge of the battery, Xie et al. [26] considered the battery discharging depth when designing the cruising strategy of PHEVs. However, the road slope was ignored in their studies. In this paper, we propose a hierarchical energy-oriented cruising controller for a four-wheel independent drive (4WID) EV on highways with varying slopes. At the upper level, the driving speed profile is optimized using DP, and then, the energy management algorithm at the lower level is designed to decide the torque allocation between the front and rear wheels. It should be noted that in addition to energy efficiency improvements, battery aging is also considered because varying charge and discharge rates may reduce the battery life.

The contribution of this paper is as follows: First, an energy-oriented cruising control strategy for EVs on highways with varying slopes is proposed based on DP while considering energy efficiency and battery aging simultaneously. The best driving pattern achieving a balance between efficiency and battery life is analyzed. Second, an enhanced eco-cruising considering lead vehicles is presented by incorporating the look-ahead controller. Third, the vehicle speed trajectory and energy management of EVs are integrated in this paper to achieve the co-optimization of vehicle longitudinal and powertrain control.

The remainder of this paper is organized as follows: Sect. 2 presents the vehicle dynamics and eco-cruising problem formulation. The hierarchical energy-oriented cruising controller, including the speed profile optimization and energy management, is introduced in Sect. 3. The control in the car-following scenario is also presented. In Sect. 4, the simulation results of the energy-oriented cruising control on highways with varying slopes are discussed. Sect. 5 concludes the paper.

2 Dynamics modeling

The concept of energy-oriented cruising control on highways with varying slopes is depicted in Figure 1. By using the Global Positioning System (GPS) and a precise digital map, the host vehicle can obtain its current position and road gradient information in the future horizon. By incorporating the received information with the vehicle dynamics, the energy-oriented controller optimizes the vehicle speed and generates the proper motor torque by minimizing the energy consumption over the whole travelling distance under given safety constraints. In addition, since the host vehicle drives in sparse traffic without considering the connection to the lead vehicles, the global optimization strategy is also useful in terms of energy savings and achieves the best optimization result over the whole route. This paper will focus on designing an energy-oriented cruising controller for EVs with

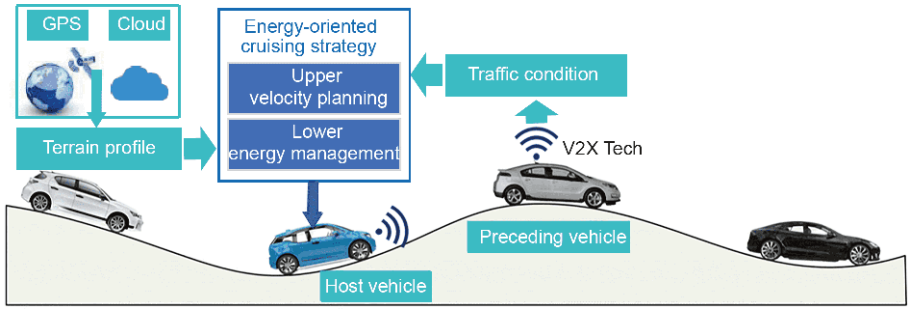

Figure 1 (Color online) Energy-oriented cruising control on highways with varying slopes.

four in-wheel motors (IWMs). The main vehicle and powertrain parameters of this EV model are listed in Table 1.

2.1 Vehicle longitudinal dynamics

The resistance of the vehicle is composed of the rolling resistance F_γ, aerodynamic resistance F_ω, gradient resistance F_θ, and inertial resistance F_α, as depicted in Figure 2 and shown in eq. (1), where the driving power P_e is achieved by 4 IMWs; g is the gravity factor; m and A_f are the vehicle mass and frontal area, respectively; v is the instantaneous vehicle speed; θ is the grade of the road; and C_γ, C_ω and ρ_α represent the resistance coefficients. To establish a direct mapping between vehicle speed and traveling distance, the dynamics (1) are converted into the spatial domain when $v>0$, i.e.,

$$\begin{aligned}\frac{p_e}{v} &= F_\gamma + F_\omega + F_\theta + F_\alpha \\ &= mgC_\gamma\cos\theta + \frac{1}{2}C_\omega\rho_\alpha A_f v^2 + mg\sin\theta + m\cdot a,\end{aligned} \tag{1}$$

$$\begin{aligned}\frac{d_v}{d_s} &= \frac{1}{v}\cdot a \\ &= \frac{1}{v}\cdot\left(\frac{p_e}{v} - gC_\gamma\cos\theta - \frac{1}{2m}C_\omega\rho_\alpha A_f v^2 - g\sin\theta\right).\end{aligned} \tag{2}$$

2.2 In-wheel motor model

The IMW in this paper is modeled as a quasi-static model, where the energy efficiency η_e is a function of its speed ω_m and torque T_m. The maximum torque of an IMW under different speeds is limited by its maximum power. Figure 3 shows the efficiency map of the IWM. In addition, the energy consumed or regenerated by the IWM, p_m, can be calculated by

$$p_m = T_m\omega_m\eta_e^k, \tag{3}$$

where the exponent k represents the state of the IWM, i.e., the motor or generator. k=1 when the torque of the IWM is positive and the battery is discharged, and k=–1 when the torque is negative.

Table 1 Nominal Parameters of 4-IWM EV model

Component	Parameter	Symbol	Value
Vehicle	Mass	M	1520 kg
	Tire radius	R_{tire}	0.3 m
	Frontal area	A_f	2.2 m^2
IWMs	Maximum power	p_e	12 kw
	Maximum torque	$T_{\max}$	300 N m
	Maximum speed	$n_{\max}$	1500 r/min
Battery	Pack capacity	E_b	24 kW h
	Voltage	V_{oc}	365 V
	Heat transfer area	A_t	1.5 m^2
	Mass	m_b	280 kg

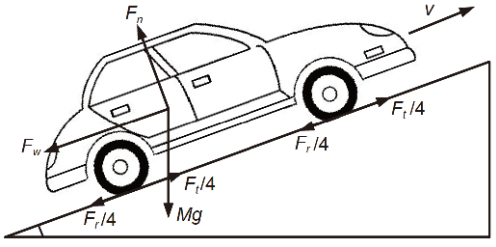

Figure 2 Vehicle longitudinal dynamics on ramp.

2.3 Battery dynamics

The battery is an essential component of an EV and greatly influences the energy management of the EV.

The $LiFePO_4$ battery is modelled as an equivalent circuit model, which governs the battery dynamics by

$$\frac{d_{\text{SOC}}}{d_s} = -\frac{i_{\text{batt}}}{Q_{\text{batt}}} = -\frac{V_{\text{oc}} - \sqrt{v_{\text{oc}}^2 - 4p_{\text{batt}}R_{\text{int}}}}{2Q_{\text{batt}}R_{\text{int}}}, \tag{4}$$

where i_{batt} is the current of charging or discharging, $C_{b\_\max}$ is the battery capacity, and V_{oc} and R_{int} are the open-circuit voltage and internal resistance of the battery, which are related to the level of SOC. The battery power p_{batt} is positive during discharging and negative during charging.

To prevent the decay of the battery life from frequent

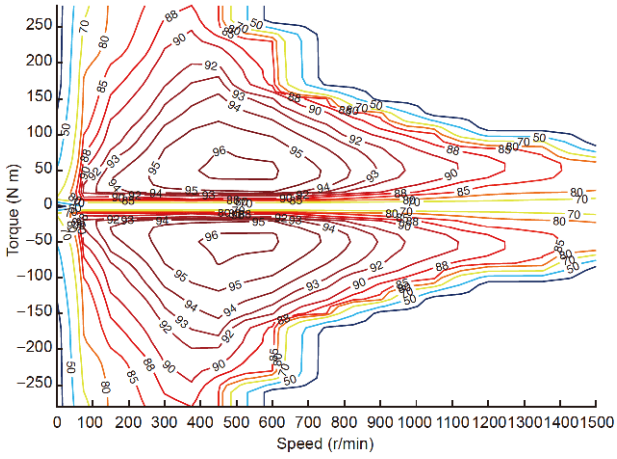

Figure 3 (Color online) Efficiency map of IWM.

charge-discharge operations, an accurate understanding of battery SOH is required. Numerous battery SOH models have been formulated to capture the relevant aging mechanisms [27–30]. For example, a first-principles-based model presented by Ramadass was developed by incorporating a continuous occurrence with a solvent reduction reaction [27]. The effect of porous electrodes on battery fade is also considered [28]. The electrochemical model can capture the aging dynamics precisely; however, its heavy computational burden makes it infeasible for practical applications [29]. Since the discharge/charge rate, temperature, and depth of discharge (DOD) have been identified as the main causes of the aging of batteries, a semi-empirical model based on experimental data is used here to evaluate the battery life in this paper [30].

$$Q_{\text{loss}} = B(I_c) \cdot \exp\left(\frac{-E_a(I_c)}{R \cdot T_b}\right) \cdot (A_h)^z, \tag{5}$$

where $B(I_c)$ is the impact factor determined by the instantaneous discharge rate of the battery I_c based on the experimental data, as shown in Table 2, where I_c=1 represents a discharge/charge current of the battery equal to 2 A. A_h is the discharge/charge Ah-through-flow,and T_b is the absolute temperature of the battery. The ideal gas constant R and exponential factor z are constant, equal to 8.31 and 0.55, respectively. $E_a(I_c)$ is the activation energy calculated by

$$E_a = 31700 - 370.3 \cdot I_c. \tag{6}$$

The battery capacity loss Q_{loss} with respect to its initial value can be estimated by

$$\frac{dQ_{\text{loss}}}{d_s} = \frac{I_c}{v} \cdot zB(I_c) \cdot \exp\left(\frac{-E_a(I_c)}{R \cdot T_b}\right) \cdot (A_h)^{z-1}. \tag{7}$$

Figure 4 shows the effects of the temperature and discharging rate on the SOH. These figures indicate that an

Table 2 Initial constant factor corresponding to I_c

I_c	$B(I_c)$
0.5	31630
2	21681
6	12934
10	15512

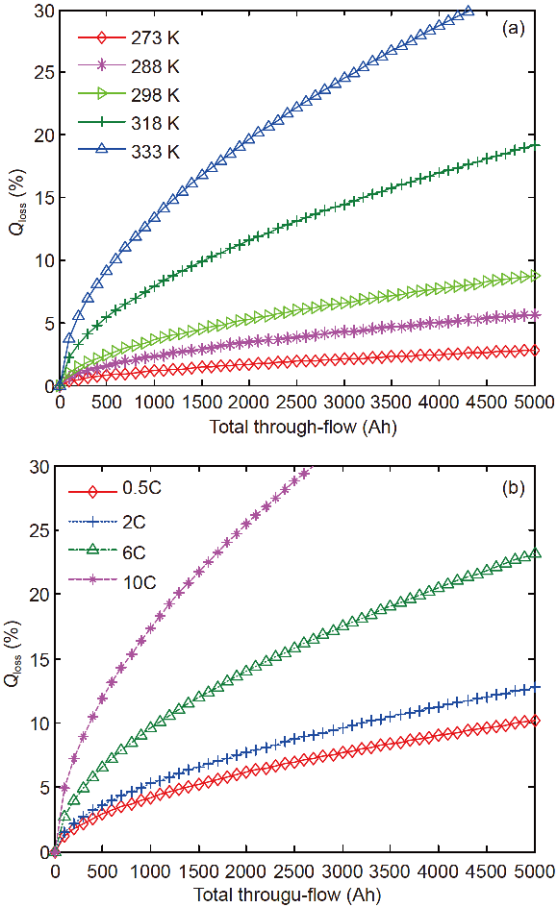

Figure 4 (Color online) The effect of temperature and discharging rate on the SOH. (a) Effect of temperature; (b) effect of discharging rate.

operating temperature under 298 K (25°C) and a lower discharging rate are beneficial to extending battery life. It should be noted that the battery is assumed to be at its end of life (EOL) when the battery capacity has decreased by 20 % from its normal value.

3 Energy-oriented cruising controller design

This section focuses on designing a hierarchical energy-saving cruising controller for four-wheel independent drive (4WID) EVs on highways with varying slopes. The goal of this controller is to obtain proper front and rear motor torque (T_{mf} and T_{mr}) profiles to improve the EV's energy efficiency

and prolong the battery life simultaneously. Thus, the optimal control problem is formulated as

$$\min J = \int_{s_o}^{s_f} [P_{\text{batt}}(T_{mf}, T_{mr}) + \alpha Q_{\text{loss}}(T_{mf}, T_{mr}, T_b)]\mathrm{d}s, \tag{8}$$

subject to

$$\frac{d_v}{d_s} = \frac{1}{mv} \cdot a = \frac{1}{v} \cdot \left(\frac{p_e}{v} - mgC_\gamma \cos\theta - \frac{1}{2} C_\alpha \rho_\alpha A_f v^2 - mg\sin\theta \right),$$

$$\frac{d_{\text{SOC}}}{d_s} = -\frac{V_{oc} - \sqrt{v_{oc}^2 - 4p_{\text{batt}} R_{\text{int}}}}{2Q_{\text{batt}} R_{\text{int}}},$$

$$\frac{dQ_{\text{loss}}}{d_s} = \frac{I_c}{v} \cdot zB(I_c) \cdot \exp\left(\frac{-E_a(I_c)}{R \cdot T_b} \right) \cdot (A_h)^{z-1},$$

$$T_{\min}(\omega_{mf}) \le T_{mf} \le T_{\max}(\omega_{mf}),$$

$$T_{\min}(\omega_{mr}) \le T_{mr} \le T_{\max}(\omega_{mr}),$$

$$v_{\text{road\_min}} = v_{\min} \le v \le \min(v_{v\_\max}, v_{\text{road\_max}}),$$

$$a \le a_{\text{limit}},$$

$$I_{b\_\min} \le I \le I_{b\_\max},$$

$$\text{SOC}_{\min} \le \text{SOC} \le \text{SOC}_{\max},$$

where α is a weighting factor and $v_{\min}$ and $v_{\max}$ are the lower and upper bounds of vehicle velocity, respectively. Note that the maximum speed is determined by the speed limit of the road. The limitation on the acceleration a_{limit} is designed for avoiding poor driving comfort. $I_{b\_\min}$ and $I_{b\_\max}$ are the bounds of the maximum charging and discharging current of the battery cell. To solve the optimal control problem (8), this energy-oriented cruising control strategy converts the optimization of T_{mf} and T_{mr} into two layers, i.e.,

Upper Layer: optimize the vehicle speed profile (equivalent to optimizing the vehicle torque demand T_{dem}) to minimize the cost function.

Lower Layer: toque allocation between the front and rear wheels to achieve optimal energy efficiency.

3.1 Speed profile optimization

The goal of the upper layer control is to obtain the optimal vehicle speed profile within a given variable velocity range by using a global optimal control method: dynamic programming (DP). The DP technique is a numerical method used to solve complex problems by dividing the optimization problem into various simpler sub-problems based on Bellman's principle. After solving all the generated sub-problems, the optimal solution of the entire problem can be computed by minimizing the cost function at each time step recursively.

Discretizing the problem in the time domain is less appropriate because the time durations vary under different speed profiles, which results in different numbers of sampling steps. To implement the DP, the same number of sampling steps is required. Therefore, in this paper, instead of discretizing the problem in the time domain, the optimal control problem is solved in a discrete-distance format as shown in

$$\min_{u \in U} J = \sum_{K=0}^{N-1} [P_{\text{batt}}(P_{\text{batt}}(x(k), u(k)) + \alpha Q_{\text{loss}}(x(k), u(k)) \cdot \Delta s(k), \tag{9}$$

subject to

$$T_{\min} \le T_{\text{dem}}(k) \le T_{\max},$$

$$v_{\text{road\_min}} = v_{\min} \le v \le \min(v_{v\_\max}, v_{\text{road\_max}}),$$

$$a \le a_{\text{limit}},$$

$$I_{b\_\min} \le I \le I_{b\_\max},$$

where $\Delta s(k)$ is the distance in each sampling step. Assuming constant acceleration and deceleration in each sampling interval, the time duration is

$$\Delta s(k) = \frac{2\Delta t}{v(k+1) + v(k)}. \tag{10}$$

In this problem, the state variables $x(k)$ are the vehicle speed, and the control variable is the total torque provided by the four IWMs, which is also referred to as the vehicle torque demand T_{dem}.

The optimal control problem in eq. (9) is divided into various simpler sub-problems, as shown in eqs. (11) and (12), where $G(x(N))$ is the terminal cost function determined by the terminal states and $J_k^*(x(k))$ is the optimal cost function at state $x(k)$ starting from time stage k.

The high nonlinearity of the introduced system dynamics makes it difficult to solve each sub-problem in DP analytically. Instead, in this paper, we use quantization and interpolation to discretize the optimal control problem into finite grids and solve it numerically [31]. It should be noted that the cost function $J_k^*(x(k))$ at each stage is only calculated at the grid points of the states. Thus, when the next state $x(k+1)$ does not fall on the determined grid point, as shown in Figure 5, $J_{k+1}^*(x(k+1))$ in eq. (12) should be calculated by an interpolation technique.

Step $N-1$,

$$J_{N-1}^*(x(N-1)) = \min_{u \in U} [(p_{\text{batt}}(x(N-1), u(N-1)) + \alpha Q_{\text{loss}}(x(N-1), u(N-1)) \cdot \Delta t(N-1) + G(x(N))], \tag{11}$$

Step $k, 0 \le k < N-1$,

$$J_k^*(x(k)) = \min_{u \in U} [(p_{\text{batt}}(x(k), u(k)) + \alpha Q_{\text{loss}}(x(k), u(k)) \cdot \Delta t(k) + J_{k+1}^*(x(k+1))]. \tag{12}$$

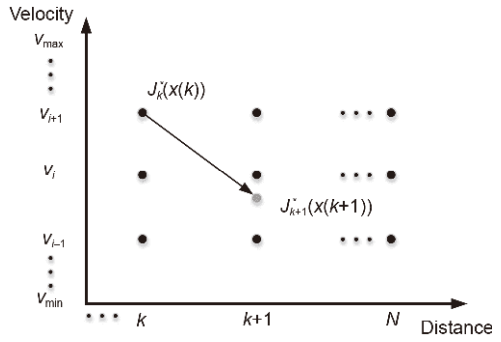

Figure 5 The discrete distance of the DP implementation.

3.2 Torque allocation optimization

The upper layer of the energy-saving controller can obtain the optimal vehicle velocity profile along the route by applying the resulting energy-oriented optimal control rule, i.e., the torque demand of the vehicle with the highest efficiency. In 4WID EVs, the overall energy efficiency can be further improved by tuning the torque split between the front and rear wheels [32–34]. As a special case, under certain extreme conditions, using one of the driving shafts to drive and the other one to recover energy by regenerative braking is more efficient than an even torque split [34]. Therefore, in this subsection, a torque allocation optimization strategy is proposed to achieve more efficient vehicle operation.

It is assumed that the EV is traveling on a road with good conditions and that the rotation speeds of all four wheels are equal. The goal of the energy management is to find the torque allocation coefficients of the front and rear wheels k_f and k_r to minimize the energy consumption while meeting the optimized speed level or a given torque demand T_{dem}. Thus, the energy optimization problem is shown as follows:

$$\begin{aligned} &\min_{k_f,k_r} J_{\text{EMS}} = k_f T_{\text{dem}} \cdot \omega_f \cdot \eta_f^{k_1} + k_r T_{\text{dem}} \cdot \omega_r \cdot \eta_f^{k_2}, \\ &k_f + k_r = 1, \end{aligned} \tag{13}$$

where J_{EMS} is the overall energy consumption of the vehicle, including both driving and regenerative braking modes. The rotational speed of the front wheel ω_f is equal to the rear wheel's ω_r. η_f and η_r are the corresponding efficiencies of the IWMs. The exponents k_1 and k_2 are equal to –1 when the IWM is being utilized for driving and 1 when the IWM is performing regenerative braking.

3.3 Controller design for car following

The derived optimal control rule can be applied to EVs for efficient cruising on highways without traffic. However, the energy-oriented cruising may be impeded by preceding vehicles in the real world. In this subsection, we present a proper traffic model with preceding vehicles and discuss the energy-oriented cruising strategy design in a car-following scenario to achieve both improved efficiency and driving safety.

To prevent potential rear-end collisions, the preceding vehicle should represent a constraint. Here, the distance between two cars $\Delta d(k)$ is calculated by

$$\Delta d(k) = d_p(k-1) + v_p(k) \cdot \Delta t(k) - (d_h(k-1) + \Delta s), \tag{14}$$

where $d_p(k-1)$ and $d_h(k-1)$ are the position of the preceding vehicle and the host vehicle at stage k−1, respectively. To distinguish whether the varying following distance $\Delta d(k)$ poses a danger to the two vehicles, a concept called the safety distance d_f is proposed, and the mathematical expression is given by

$$d_f = \lambda \cdot d_{\min} = \lambda \cdot \frac{m \cdot v_h^2}{2 \cdot F_{t\_\max}}, \tag{15}$$

where $d_{\min}$ is the shortest braking distance for a speed of v_h, λ is a margin of safety, and m and $F_{t\_\max}$ are the vehicle mass and the maximum longitudinal brake force acting on the vehicle by the tire, repesctively. Three rules are listed in eq. (16) to ensure the safety of the car-following scenario while avoiding rear-end collisions. The car-following scenario and the respective formulas are shown in Figure 6.

$$v(k+1) = \begin{cases} v_{\text{opt}}, & \Delta d_k > d_f, \\ v_k - a_c \cdot \Delta t_k, & d_{\min} < \Delta d_k \le d_f, \\ -a_{\max} \cdot \Delta t_k, & \Delta d_k \le d_{\min}, \end{cases} \tag{16}$$

where v_{opt} is the optimal velocity calculated in the eco-driving strategy and a_c and $a_{\max}$ are the maximum deceleration without producing discomfort to the vehicle's occupants and the maximum deceleration of the vehicle, respectively.

4 Simulation and discussion

To validate the performance of the proposed controller, a city expressway is selected near Laoshan, Nanjing, for the cruising simulation, as shown in Figure 7. The longitude, latitude, distance and altitude information are obtained from Google. The route is approximately 4000 m, and its terrain profile is shown in Figure 7.

4.1 Simulation results of highway cruising

Before using DP to derive the optimal cruising velocity, the grid sizes of the distance, states and controls, which affect the accuracy and computation time of DP, should be decided first. A large sampling step will generate poor optimization results, while a small sampling step will increase the computation time. In this paper, the entire route is discretized by Δs of 25 m, and the grid sizes of the velocity and torque

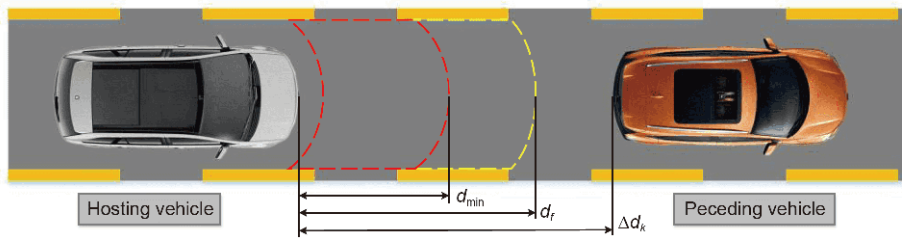

Figure 6 (Color online) Car-following scenario.

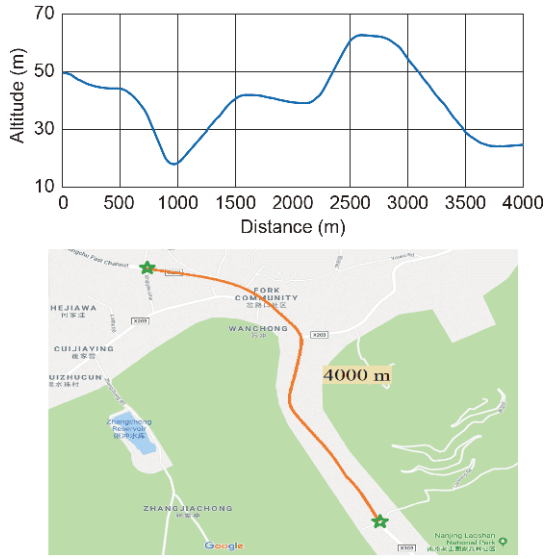

Figure 7 (Color online) Terrain profile of selected real road route.

demands are 0.5 m/s and 2 N m, respectively. The speed limit of this road is 90 km/h, and the speed range is set to 70–90 km/h. The initial battery SOC for all cases is 0.8. In addition, it is assumed that the vehicle is a new vehicle; thus, the initial battery capacity loss is zero.

4.1.1 Tradeoff between energy consumption and battery aging

When increasing the weighting factor α in the cost function, the EV's energy consumption will increase and the battery life will be prolonged in the simulation. The changes in the energy consumption and battery capacity loss with increasing weighting factor α are depicted in Figure 8 (a), where the x axis is the weighting factor. From data points 4 to 6, we can see that a small increase in energy consumption can achieve a large battery life improvement. To achieve a tradeoff between energy efficiency and battery life, we choose data point 7 in Figure 8(a), which is marked in red in Figure 8(b), showing the results of the energy consumption and battery capacity loss under different weighting factors.

4.1.2 Comparison with constant speed cruising

Using the energy-oriented cruising strategy introduced in Sect. 3, the optimal vehicle velocity profile and the torque distributions are derived. Figure 9 shows the simulation results for a constant velocity of 75 km/h and varying-vehicle-velocity cruising strategies (between 70 and 90 km/h) with α=0 and the optimal α. The α=0 scenario represents the objective function without considering battery aging, and the optimal α scenario represents the objective function that achieves a tradeoff between energy consumption and battery life derived in the last subsection. Compared to the strategies using variable speeds, the constant-speed cruising shows a worse performance in terms of both energy efficiency and battery life since it cannot change the torques in a flexible manner due to the lack of prediction ability as the terrain slope varies.

For the strategy not considering battery aging (α=0), the variations of the vehicle speed present the following features. First, the vehicle continues cruising at a speed close to the minimum speed limit since lower speeds require less energy to overcome air resistance. Second, the vehicle is accelerated before the steep uphill terrain to make full use of the kinetic energy during uphill climbing, e.g., at 800–1000 and 2100–2300 m in Figure 9.

For the strategy with optimal α, the varied speed follows a similar trend as the strategy with α=0, i.e., accelerating before the steep uphill terrain and decelerating during uphill climbing; however, a larger amplitude is observed. Larger variations in speed make the vehicle torque demand smother than under the constant speed and (α=0) strategy, as shown in Figure 9, resulting in the lower current flowing through the battery and reduced battery capacity losses in Figure 9.

Table 3 shows the average speed, energy consumption, and battery capacity loss of different cruising strategies and with constant-speed driving, where the average speed refers to the average speed during the entire route, therein reflecting the travel time cost. The constant-speed cruising at 70 km/h is taken as the benchmark. The strategy with α=0 shows a 5.26% energy consumption reduction and a 21.86% battery life improvement over the 70 km/h cruising strategy. Compared to constant-speed cruising, the varying velocity strategy will result in efficient vehicle operation and a longer battery life. By adding the penalty of the battery capacity loss, the strategy with optimal α makes a concession on energy efficiency to achieve a two-fold increase in battery

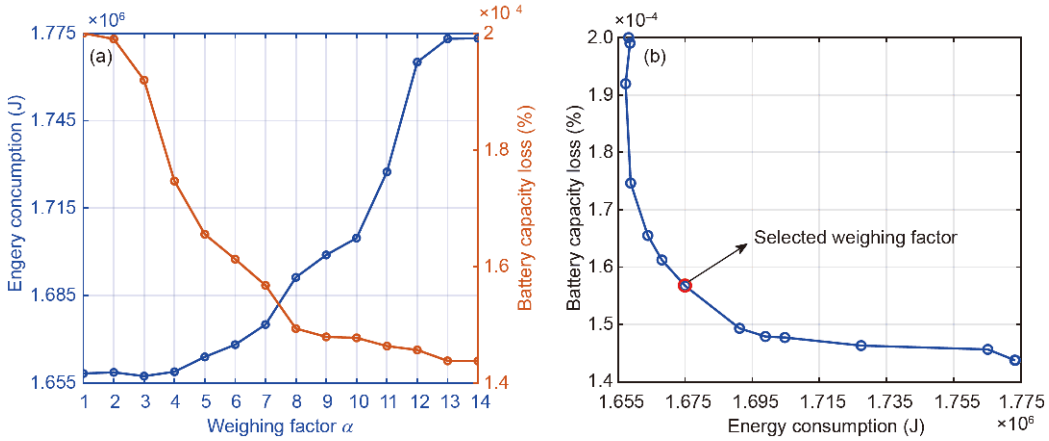

Figure 8 (Color online) Energy consumption and battery capacity loss under different weighing factors α. (a) Energy consumption and battery capacity loss trend; (b) tradeoff between energy consumption and battery capacity loss.

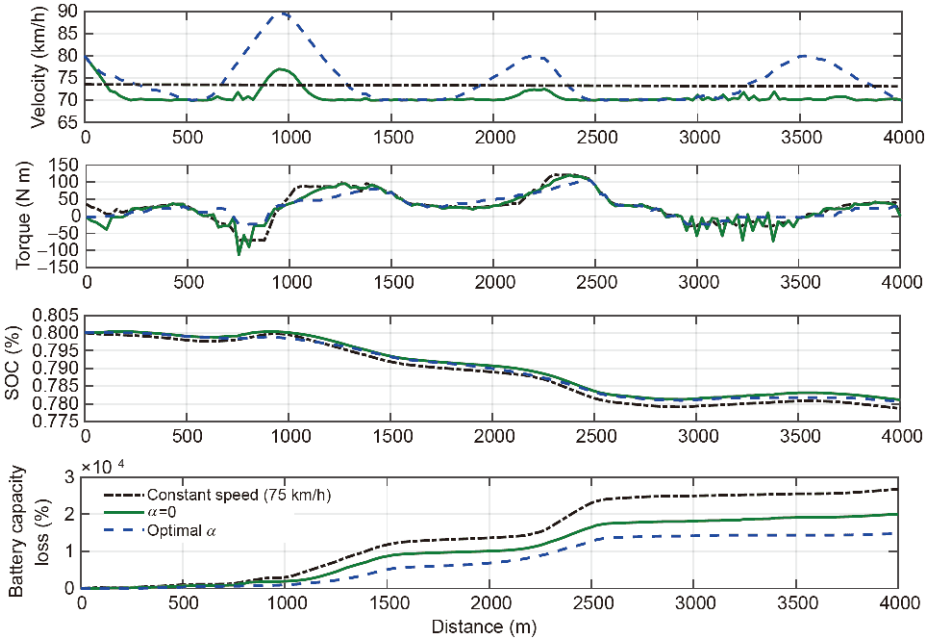

Figure 9 (Color online) Comparison of torque distributions, SOC and SOH between constant-speed and varying vehicle velocity strategy with α.

Table 3 Comparison of simulation results

Strategy	Average speed (km/h)	Energy consumption (J)	Improvement	Battery capacity loss (%)	Improvement
Constant speed	70	1.7502×10^{6}	Benchmark	2.5614×10^{-4}	Benchmark
	75	1.8733×10^{6}	–7.03%	2.6771×10^{-4}	–4.52%
$\alpha = 0$	70.8	1.6582×10^{6}	5.26%	2.0016×10^{-4}	21.86%
Optimal α	74.3	1.6989×10^{6}	2.95%	1.4789×10^{-4}	42.26%

life compared to the strategy with α=0 while reducing the travel time due to the higher travel speed.

Table 4 shows the energy efficiency improvement of the hierarchical controller compared to the single-level controller without optimal torque allocation between the front and rear axles. The designed lower level controller, i.e., the optimal torque allocation strategy, achieves 2.25% and 2.47% energy savings during constant-speed and varied-speed cruising, respectively. Moreover, the energy consumption reduction also extends the battery life, as the am-

pere-hours flowing through the battery shown in eq. (4) are reduced.

4.1.3 Effect of speed range and level on energy efficiency and battery life

The selection of the speed range and average speed can significantly affect the energy consumption and battery life. Thus, in this subsection, we simulate the proposed energy-oriented cruising strategy with different ranges (i.e., +/–5, 10 and 15 km/h) and different levels of average speed (i.e., 40, 50, 60, 70, and 80 km/h).

The simulation results are shown in Figure 10. When increasing the average speed from 40 to 80 km/h, the energy consumption and battery capacity loss both increase. This is because at higher average speeds, the vehicle needs more energy to overcome the resistance caused by air friction. Greater energy consumption leads to higher ampere-hours flowing through the battery, as shown in eq. (4), resulting in greater battery capacity losses. On the other hand, a larger speed range is beneficial to both energy efficiency and battery life because the speed limit is a constraint in the optimal control problem. By relaxing the constraint, the system has greater freedom to drive the vehicle in a more efficient area and achieve a longer battery life. It should be noted that the average speed has a greater influence on the energy consumption than does the battery life when using the proposed controller, while greater battery life improvements can be achieved by increasing the size of the speed range.

4.2 Car-following scenario

In the simulation of the car-following scenario, the host vehicle applied the energy-oriented cruising strategy within the speed range of 70–90 km/h. A preceding vehicle is cruising at a constant speed of 72 km/h and cuts into the host vehicle's lane 100 m ahead.

The resulting velocity profiles of the host car and preceding car are drawn in Figure 11(a), which also gives the velocity of a free car driving with its energy-optimal strategy. The host vehicle is restricted by the preceding vehicle, and the spacing between them approximates the preset safety distance, as shown in Figure 11(b). The velocity profile of the host vehicle deviates from the optimum to prevent a possible rear-end collision. In this case study, the energy consumption and battery capacity losses of the following vehicle increase by 12.8% and 15.4%, respectively, compared with the free cars. However, the energy efficiency and battery life are still improved compared to the constant-speed strategy in this case.

5 Conclusions

This paper presents a hierarchical energy-oriented cruising control strategy for 4WID EVs on highways with up-down slopes. In the upper layer, the optimally varied vehicle velocity is calculated using DP, which takes both energy effi-

Table 4 Improvement of hierarchical controller with TCA

Category		Energy consumption (J)	Improvement	Battery capacity loss (%)	Improvement
Constant speed	Single level	1.7896×10^{6}	2.25%	2.5927×10^{-4}	1.22%
	Double level	1.7502×10^{6}		2.5614×10^{-4}	
Varying speed	Single level	1.7409×10^{6}	2.47%	1.4836×10^{-4}	0.32%
	Double level	1.6989×10^{6}		1.4789×10^{-4}	

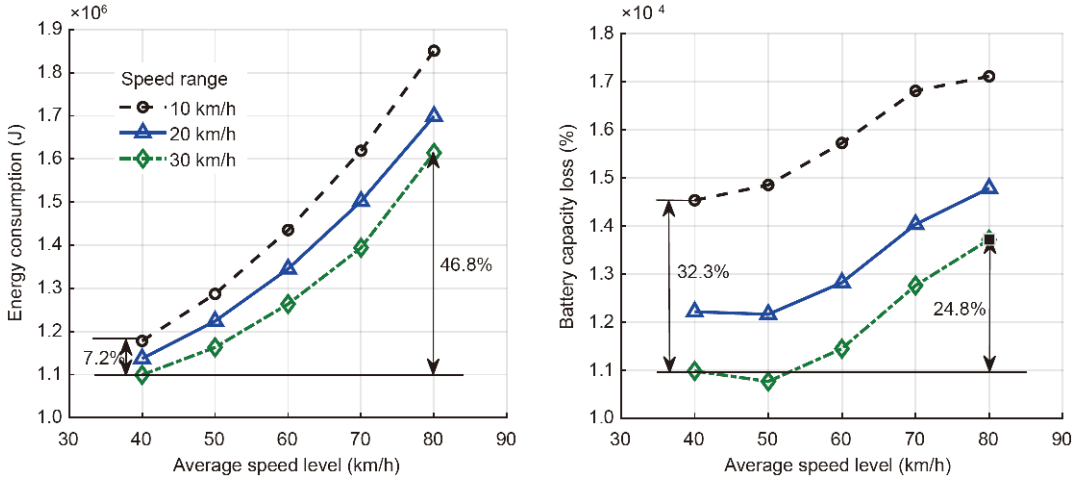

Figure 10 (Color online) Effect of the speed range and level on the SOC and battery life.

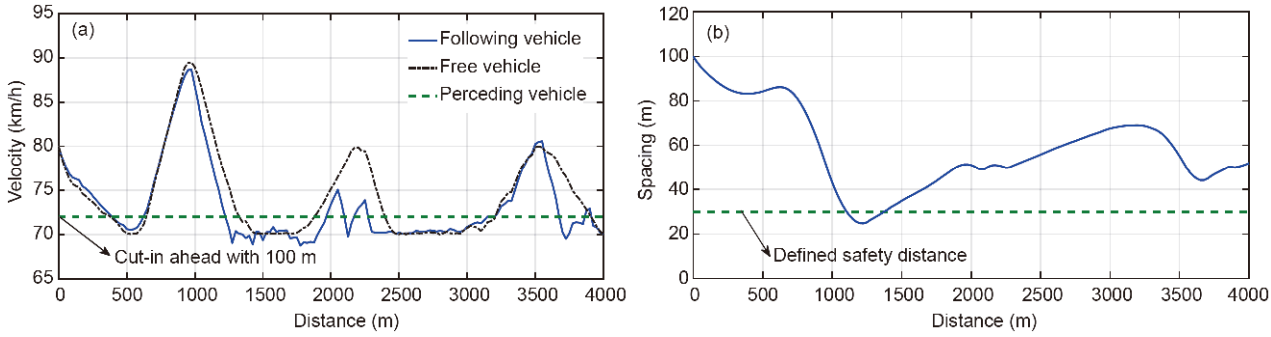

Figure 11 (Color online) Simulation results of car-following scenario. (a) Velocity profiles of following and preceding vehicles; (b) distances between preceding and following vehicles.

ciency and battery aging into consideration. In the lower layer, the torque demand derived in the upper layer is split between the front and rear axles to achieve efficient energy management. The varying vehicle velocity cruising strategy achieves a better performance than constant-speed cruising in terms of both energy efficiency and battery life. Moreover, a much longer battery life and shorter travel time can be achieved with a slight concession on energy efficiency. In addition, the car-following scenario is also simulated, therein showing considerable energy efficiency improvements and increased battery life even with preceding vehicles present.

Several prospects of future study have been planned. First, to implement the energy-optimized cruising strategy online, an instantaneous velocity optimization strategy will be designed to calculate the optimal cruising speed in real time. Second, the eco-driving strategy for HEV/EVs should be extended to urban roads, where more energy is wasted.

This work was supported in part by the National Natural Science Foundation of China (Grant Nos. 51805081, 51575103, and U1664258) and the National Key Research and Development Program in China (Grant Nos. 2016YFB0100906, and 2016YFD0700905).

1 Davis S C, Williams S E, Boundy R G. Transportation Energy Data Book: Edition 34. Energy Convers. Utili, 2015. 176: 319–338
2 Liu T, Hu X S, Hu W H, et al. A heuristic planning reinforcement learning-based energy management for power-split plug-in hybrid electric vehicles. IEEE Trans Ind Inform, 2019, doi: 10.1109/TII.2019.2903098
3 Liu T, Yu H L, Guo H Y, et al. Online energy management for multimode plug-in hybrid electric vehicles. IEEE Trans Ind Inform, 2019, 15: 4352–4361
4 Zhuang W, Zhang X, Ding Y, et al. Comparison of multi-mode hybrid powertrains with multiple planetary gears. Appl Energy, 2016, 178: 624–632
5 Ilgin Guler S, Menendez M, Meier L. Using connected vehicle technology to improve the efficiency of intersections. Transp Res Part C-Emerging Technol, 2014, 46: 121–131
6 Zhang F, Xi J, Langari R. Real-time energy management strategy based on velocity forecasts using V2V and V2I communications. IEEE Trans Intell Transp Syst, 2017, 18: 416–430
7 Hu J, Shao Y, Sun Z, et al. Integrated optimal eco-driving on rolling terrain for hybrid electric vehicle with vehicle-infrastructure communication. Transp Res Part C-Emerging Technol, 2016, 68: 228–244
8 Jin Q, Wu G, Boriboonsomsin K, et al. Power-based optimal longitudinal control for a connected eco-driving system. IEEE Trans Intell Transp Syst, 2016, 17: 2900–2910
9 Li S E, Peng H. Strategies to minimize the fuel consumption of passenger cars during car-following scenarios. Proc Institution Mech Engineers Part D-J Automobile Eng, 2012, 226: 419–429
10 Xu S, Li S E, Zhang X, et al. Fuel-optimal cruising strategy for road vehicles with step-gear mechanical transmission. IEEE Trans Intell Transp Syst, 2015, 16: 3496–3507
11 Mensing F, Bideaux E, Trigui R, et al. Trajectory optimization for eco-driving taking into account traffic constraints. Transp Res Part D-Transp Environ, 2013, 18: 55–61
12 Hellström E, Åslund J, Nielsen L. Design of an efficient algorithm for fuel-optimal look-ahead control. Control Eng Practice, 2010, 18: 1318–1327
13 Doan V D, Fujimoto H, Koseki T, et al. Iterative dynamic programming for optimal control problem with isoperimetric constraint and its application to optimal eco-driving control of electric vehicle. IEEE J Ind Appl, 2018, 7: 80–92
14 Froberg A, Hellstrom E, Nielsen L. Explicit fuel optimal speed profiles for heavy trucks on a set of topographic road profiles. SAE Technical Paper No, 2006-01-1071
15 Chen H, Guo L, Ding H, et al. Real-time predictive cruise control for eco-driving taking into account traffic constraints. IEEE Trans Intell Transp, 2018, 20: 2858–2868
16 Kamal M A S, Mukai M, Murata J, et al. Model predictive control of vehicles on urban roads for improved fuel economy. IEEE Trans Contr Syst Technol, 2013, 21: 831–841
17 Lin Q, Li S E, Du X, et al. Minimize the fuel consumption of connected vehicles between two red-signalized intersections in urban traffic. IEEE Trans Veh Technol, 2018, 67: 9060–9072
18 Kohut N, Hedrick K, Borrelli F. Integrating traffic data and model predictive control to improve fuel economy. In: Proceedings of the 12th IFAC Symposium on Control in Transportation Systems. 2009. 155–160
19 Kamal M A S, Mukai M, Murata J, et al. Ecological vehicle control on roads with up-down slopes. IEEE Trans Veh Technol, 2011, 12: 783–794
20 Wang M, Daamen W, Hoogendoorn S P, et al. Rolling horizon control framework for driver assistance systems. Part I: Mathematical formulation and non-cooperative systems. Transport Res C-Emer, 2014, 40: 271–289
21 Xu S, Li S E, Cheng B, et al. Instantaneous feedback control for a fuel-prioritized vehicle cruising system on highways with a varying slope. IEEE Trans Intell Transp, 2017, 18: 1210–1220
22 Liu T, Wang B, Yang C. Online Markov Chain-based energy management for a hybrid tracked vehicle with speedy Q-learning. Energy, 2018, 160: 544–555

23 Zhang F, Hu X, Langari R, et al. Energy management strategies of connected HEVs and PHEVs: Recent progress and outlook. Prog Energy Combust Sci, 2019, 73: 235–256
24 Xu S, Li S E, Peng H, et al. Fuel-saving cruising strategies for parallel HEVs. IEEE Trans Veh Technol, 2016, 65: 4676–4686
25 Wu X H, He X Z, Yu G Z, et al. Energy-optimal speed control for electric vehicles on signalized arterials. IEEE Trans Intell Transp Syst, 2015, 16: 2786–2796
26 Xie S, Hu X, Qi S, et al. Model predictive energy management for plug-in hybrid electric vehicles considering optimal battery depth of discharge. Energy, 2019, 173: 667–678
27 Ramadass P, Haran B, Gomadam P M, et al. Development of first principles capacity fade model for Li-ion cells. J Electrochem Soc, 2004, 151: A196
28 Spotnitz R. Simulation of capacity fade in lithium-ion batteries. J Power Sources, 2003, 113: 72–80
29 Fuller T F, Doyle M, Newman J. Simulation and optimization of the dual lithium ion insertion cell. J Electrochem Soc, 1994, 141: 1–10
30 Wang J, Liu P, Hicks-Garner J, et al. Cycle-life model for graphite-$LiFePO_4$ cells. J Power Sources, 2011, 196: 3942–3948
31 Bertsekas D P. Dynamic Programming and Optimal Control. Belmont: Athena Scientific, 1995
32 Li B, Goodarzi A, Khajepour A, et al. An optimal torque distribution control strategy for four-independent wheel drive electric vehicles. Vehicle Syst Dyn, 2015, 53: 1172–1189
33 Dizqah A M, Lenzo B, Sorniotti A, et al. A fast and parametric torque distribution strategy for four-wheel-drive energy-efficient electric vehicles. IEEE Trans Ind Electron, 2016, 63: 4367–4376
34 Chen Y, Wang J. Design and experimental evaluations on energy efficient control allocation methods for overactuated electric vehicles: Longitudinal motion case. IEEE/ASME Trans Mechatron, 2014, 19: 538–548